Electronic Supporting Information (ESI)

Facile spray drying route for mesoporous Li_3VO_4/C hollow spheres as an anode for long life lithium ion batteries

*Yang Yang[a], Jiaqi Li[a], Xinyi He[a], Jing Wang[a], Dong Sun[b], Jinbao Zhao[a]**

[a] State Key Lab of Physical Chemistry of Solid Surfaces, Collaborative Innovation Center of Chemistry for Energy Materials, College of Chemistry and Chemical Engineering, Xiamen University, Xiamen, 361005, P. R. China.

[b] Bluestone Global Technology, Inc. NewYork, USA.

*E-mail: jbzhao@xmu.edu.cn

Materials Synthesis: The mesoporous Li_3VO_4/C hollow spheres were prepared via a spray drying method and subsequent heat treatment in Ar atmosphere. In a typical synthesis, V_2O_5 of 2 mmol (0.364 g), Li_2CO_3 of 6 mmol (0.443 g), and Glucose of 0.9 g were dissolved in distilled water of 70 ml. After stirring for 1 h, the resulting clear solution (Figure S1) was spray dried by using a Buchi mini spray drier B-290 (Figure S2) at the inlet temperature of 210 ºC and outlet temperature of 140 ºC, with aspirator rate of 100 %, rotameter setting of 40 mm and pump rate of 5% (1.5 mL min^{-1}). Nitrogen was used as the drying gas. The schematic of the spray drying route is shown in Figure S2. The hollow precursors obtained by the spray drying process were annealed at 550 ºC for 7 h at a heating rate of 5 ºC min^{-1} in Ar atmosphere. The pristine Li_3VO_4 was also prepared as below: V_2O_5 of 2 mmol (0.364 g), and Li_2CO_3 of 6 mmol (0.443 g) were dissolved in distilled water of 70 ml. After stirring for 1 h, the resulting clear solution was dried in an oil-bath at 90 ºC and then annealed at 550 ºC for 7 h at a heating rate of 5 ºC min^{-1} in Ar atmosphere.

Characterization: Raman spectra were collected *via* a Raman spectroscope (HORIBA Xplora) with the 532 nm Ar-ion laser. The XRD data were collected on Rigaku miniflex 600 equipped with Cu Kα radiation. SEM images were obtained by scanning electronic microscopy (HITACHI S-4800). TEM images were investigated by high-resolution transmission electron microscopy (HRTEM, FEI TECNAI G2 F30). Thermo gravimetric analysis (TGA) was taken on Netzsch TG 209 F1 under air flow (30 ~ 700 ºC, 10 ºC min^{-1}). The nitrogen adsorption and desorption isotherms were attained using the Brunauer-Emmett-Teller (BET, Micromeritics surface area and porosity analyzer, ASAP 2020) method.

Electrochemical Measurement: The electrochemical performances of the electrodes were tested in the form of coin cell with metal lithium foil as both counter and reference electrodes. Porous polyethylene membrane was used as the separator and 1 M $LiPF_6$ in the ethylene carbonate (EC) / diethyl carbonate (DEC) (v / v = 1 : 1) as the electrolyte. The working electrode film was obtained by casting the slurry composed of active material, acetylene black, and polyvinylidene difluoride (PVDF) binder (weight ratio of 70 : 20 : 10) dispersed in N-methyl pyrrolidone (NMP) solvent onto an Cu foil followed by drying in a vacuum oven at 80 ºC overnight. Finally, the electrode was punched into circular discs and roll-pressed. The mass loading of the active material is about 0.5 - 0.8 mg cm^{-2}. The charge-discharge cycling tests were conducted on a battery cycler (Shenzhen Neware). Electrochemical impedance spectra (EIS) tests were performed on an electrochemical workstation of Solartron SI 1287 at

the frequency range from 0.1 Hz to 100 kHz. CV measurements were performed on an electrochemical workstation of Metrohm Autolab PGSTAT 302N.

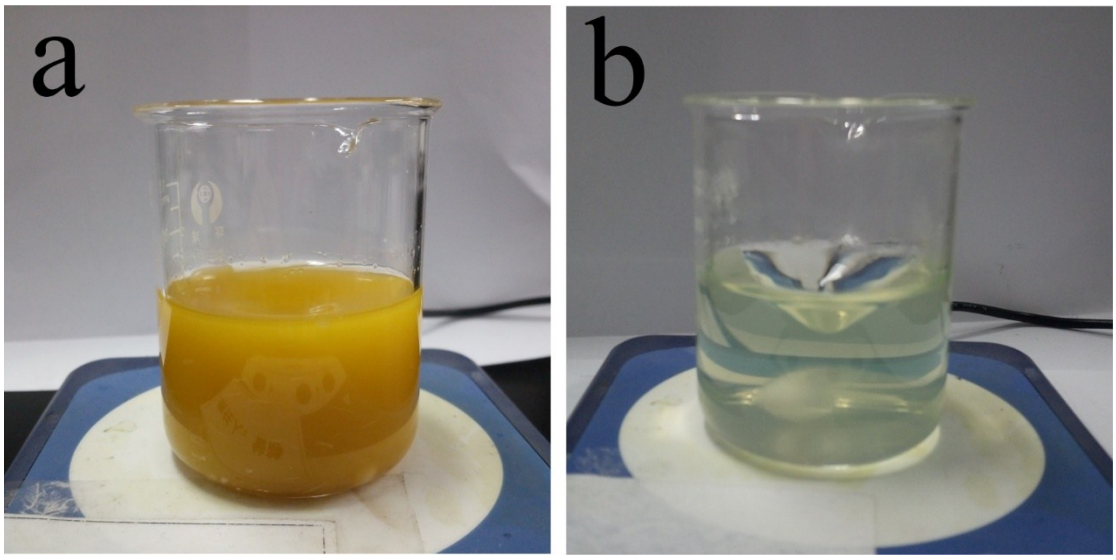

Figure S1. Photographs of the solution of Li_2CO_3 and V_2O_5 (a) before stirring; (b) stirring for 1h.

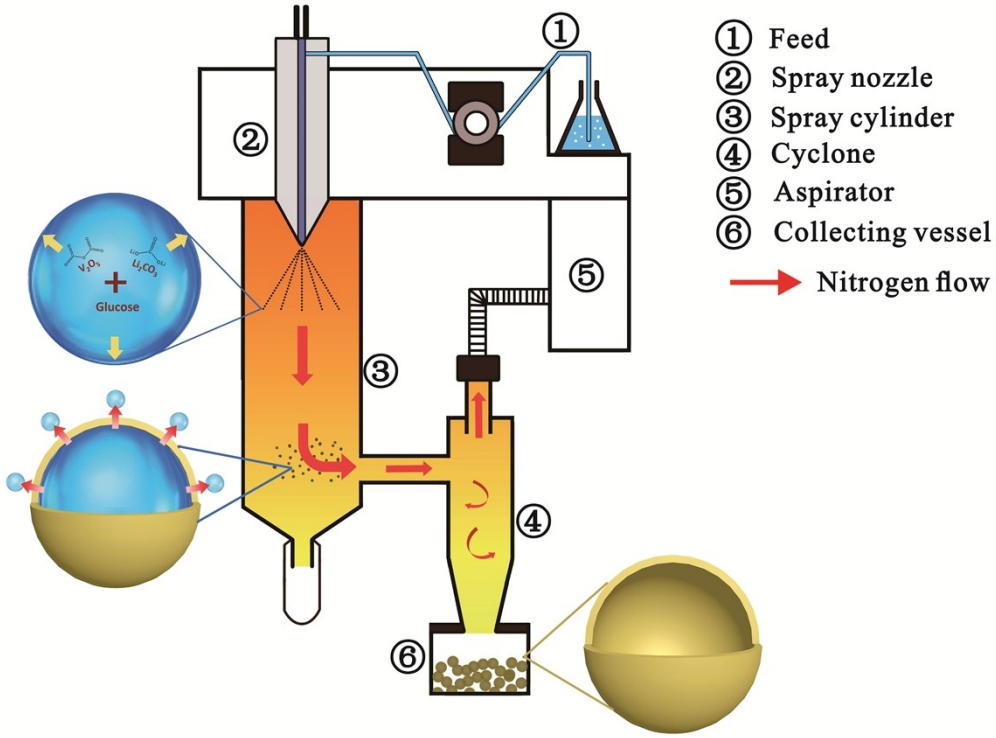

Figure S2. Schematic of the spray drying route.

The schematic of the spray drying route is shown in Figure S2. The aerosol droplets are generated from the nozzle, and then enter the droplet-to-particle conversion chamber (spray cylinder) via the carrier gas flow. Subsequently after entering the cyclone, the carrier gas is separated, and the dried particles remain in the collecting vessel. From a droplet to a dried particle, just approximately 1s is needed. Theoretically, if the drying speed of a sprayed droplet is sufficiently slow, the solute within the droplet will have sufficient time to redistribute, that will produce dense dried particles.[1] However, in our experiment, the high spray drying temperature and short residence induced by the high inlet temperature (210 ºC, which is much higher than the boil point of water) and high carrier gas flow (aspirator rate of 100%) result in fast evaporation rate. Therefore the drying of the aerosol droplet is so quick that the solute does not have adequate time to redistribute and diffuse from the surface to the center of the droplet, it accumulates near the drying front of the droplet (the external surface of the droplet that directly contacted with the hot carrier gas) instead.[2] At the end of the droplet-to-particle conversion process the evaporating front becomes a shell and form hollow structure.

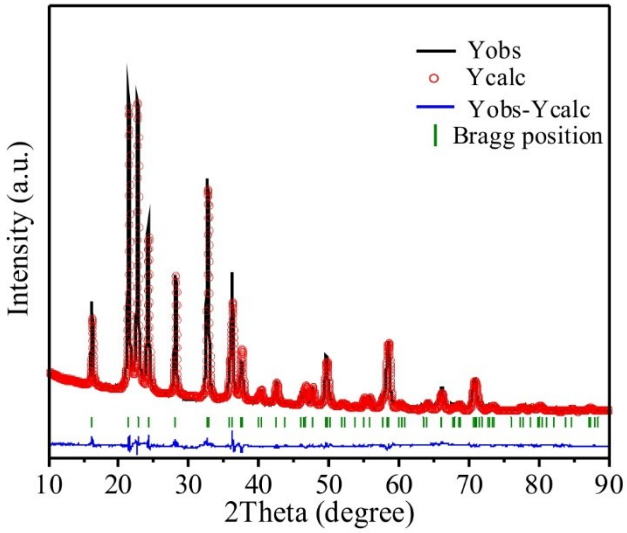

Figure S3. Rietveld analysis of LVO/C.

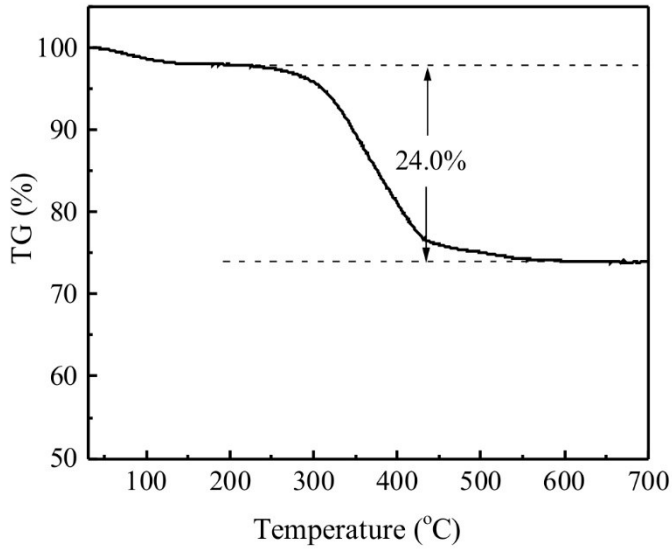

Figure S4. Thermogravimetric curve of the LVO/C.

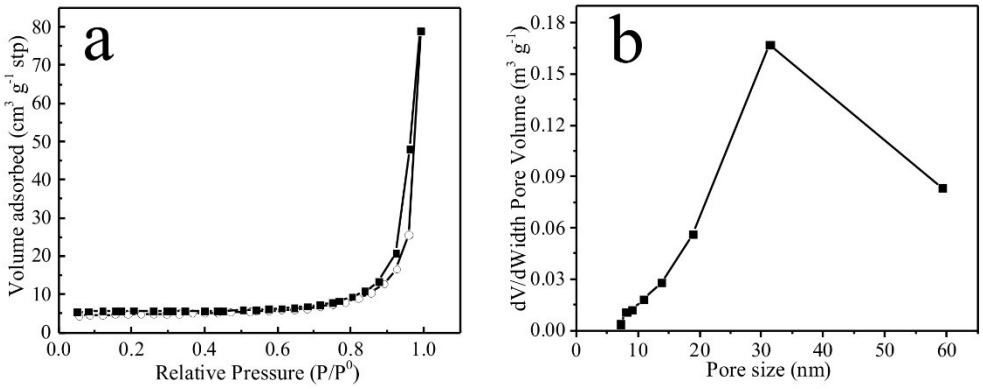

Figure S5. (a) N_2 adsorption-desorption isotherms , and (b) Pore size distribution of the LVO.

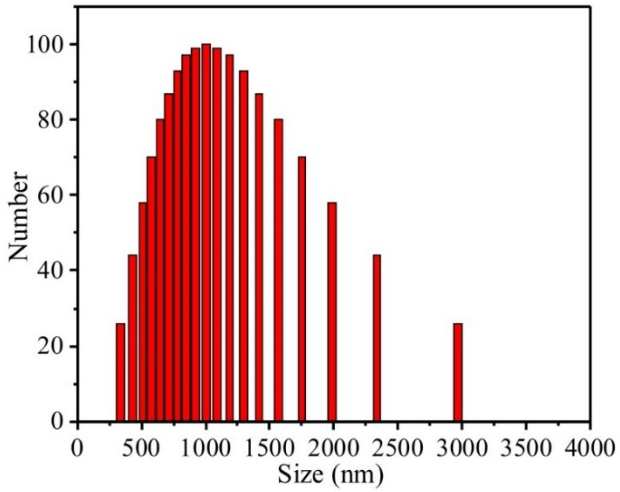

Figure S6. Particle size distribution of LVO/C.

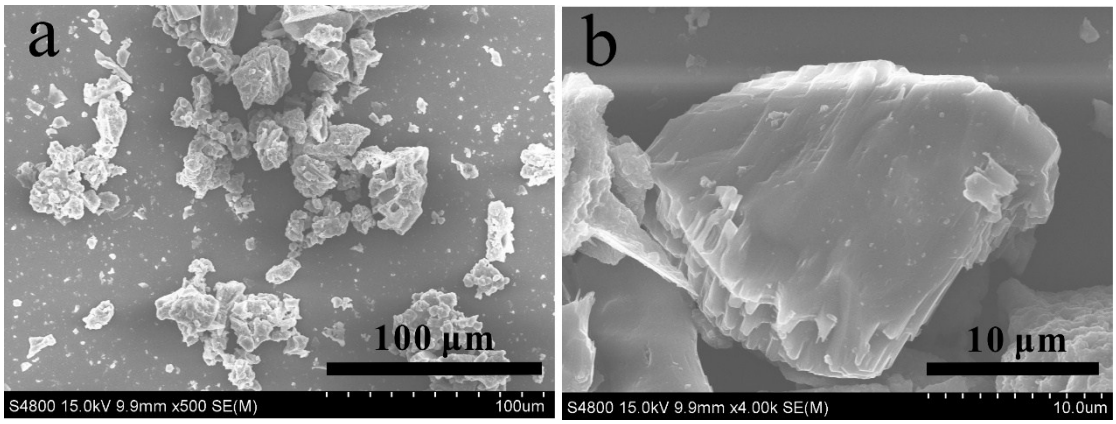

Figure S7. SEM images of the pristine LVO.

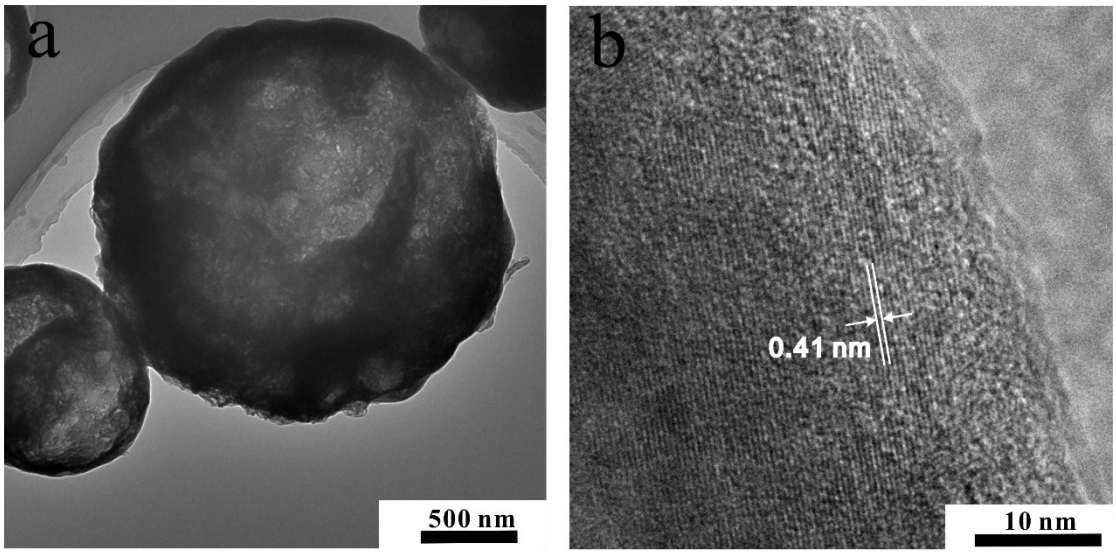

Figure S8. TEM and HRTEM images of large LVO/C particle.

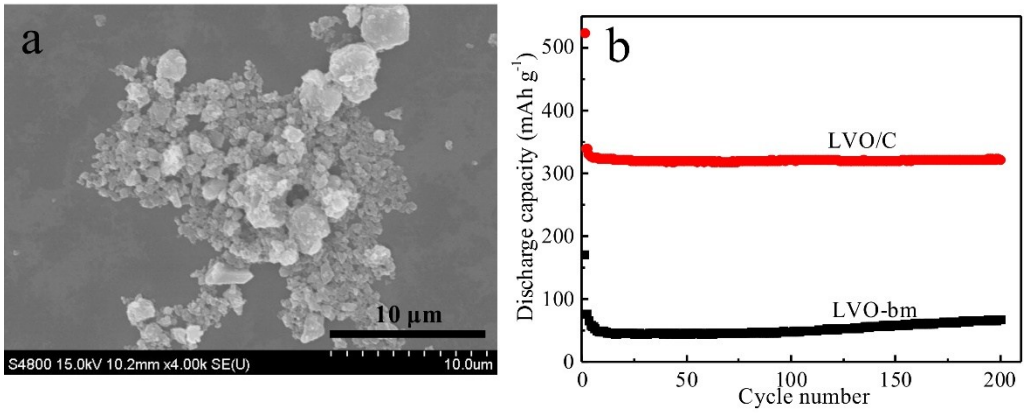

Figure S9. (a) SEM image of the LVO-bm; (b) Cycling performance of LVO-bm and LVO/C at 5 C.

The pristine LVO was ball milled in a ZrO_2 jar at a rotation speed of 400 rpm min^{-1} for 2h to obtain the LVO-bm. After ball milling, the large particles of LVO are ground into smaller irregular shaped particles with the maximum size of ~ 5 μm. The cycling performance of LVO-bm and LVO/C at 5 C is shown in Figure 3. Obviously, LVO/C still exhibits much better cycling performance than LVO-bm.

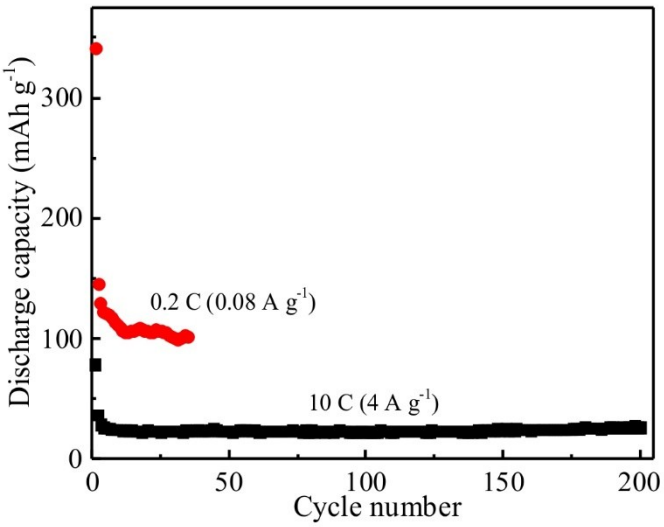

Figure S10. Cycling performance of carbon in LVO/C at 0.2 and 10 C.

Glucose was annealed at 550 ºC for 7 h at a heating rate of 5 ºC min^{-1} in Ar atmosphere to afford a carbon sample (named as C-550). C-550 exhibits discharge capacities of 102 mAh g^{-1} after 35 cycles at 0.2 C, and 27 mAh g^{-1} after 200 cycles at 10 C.

Table S1. Comparsion of the high-rate (10 C) cycling performance of the LVO/C in this work with other Li_3VO_4/carbon composite materials.

Reference	Loading of active materials (mg cm^{-2})	Cycle number	Capacity at 10 C (mAh g^{-1})
9	0.8-1.1	2000	245
12	Not mentioned	1500	257.9
13	Not mentioned	500	230
15	0.65	500	275
our present work	0.5-0.8	3000	275

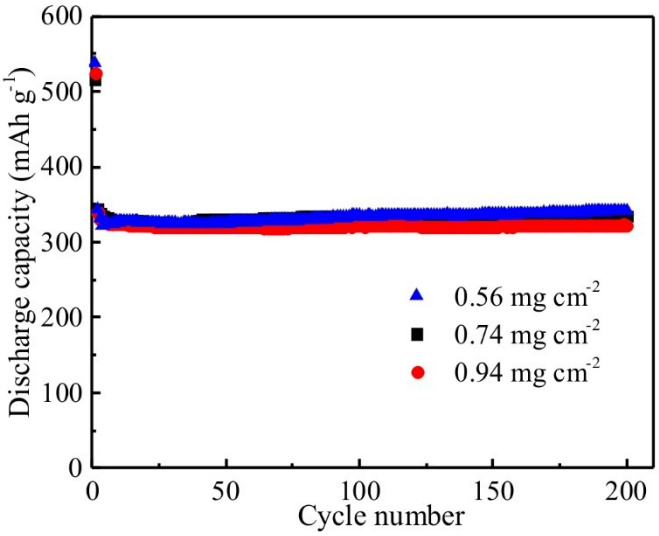

Figure S11. Cycling performance of LVO/C with different loading of active materials.

The packing density of a electrode is also very important in LIB industry. For comparing fairly the commercial graphite electrode is selected to be the comparative sample. The graphite coating is fabricated by slurry casting method as same as the LVO/C. After drying, both coatings are cut into disc-like electrodes with a diameter of 1.2 cm and subsequently pressed under a pressure of 10 MPa. The coating density and thickness of the film (containing active material, conducting agent, and binder) are measured. The packing density of electrode is calculated by the mass divided by the volume of the film.

Table S2. The packing density of LVO/C electrode.

LVO/C	Sample 1	Sample 2	Sample 3	Sample 4	Sample 5	Sample 6	Average
Coating density (mg cm^2)	1.36	1.38	1.36	1.35	1.35	1.37	
Thickness (μm)	13	13	14	14	13	14	
Packing density (g cm^3)	1.05	1.06	0.97	0.96	1.04	0.98	1.01

Table S3. The packing density of graphite electrode.

Graphite	Sample 1	Sample 2	Sample 3	Sample 4	Sample 5	Sample 6	Average
Coating density (mg cm^2)	0.95	0.94	1.00	1.07	0.99	0.96	
Thickness (μm)	10	9	9	10	9	9	
Packing density (g cm^3)	0.95	1.04	1.11	1.07	1.1	1.07	1.05

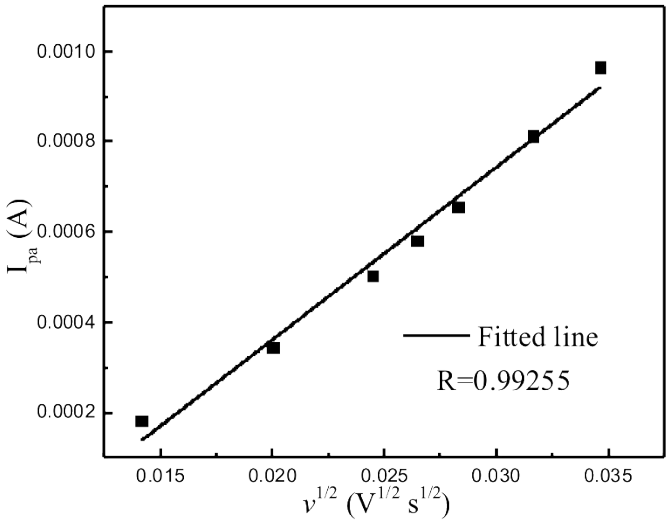

Figure S12. Dependence of oxidation peak current (I_{pa}) on the square rate of scan rate for LVO/C electrode.

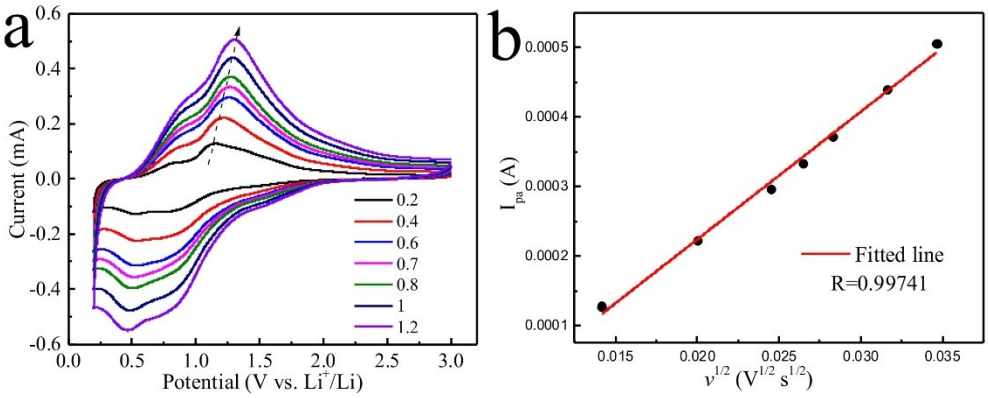

Figure S13. (a) Cyclic voltammetry curve of the LVO at different scan rates; (b) Dependence of oxidation peak current (I_{pa}) on the square rate of scan rate for LVO electrode.

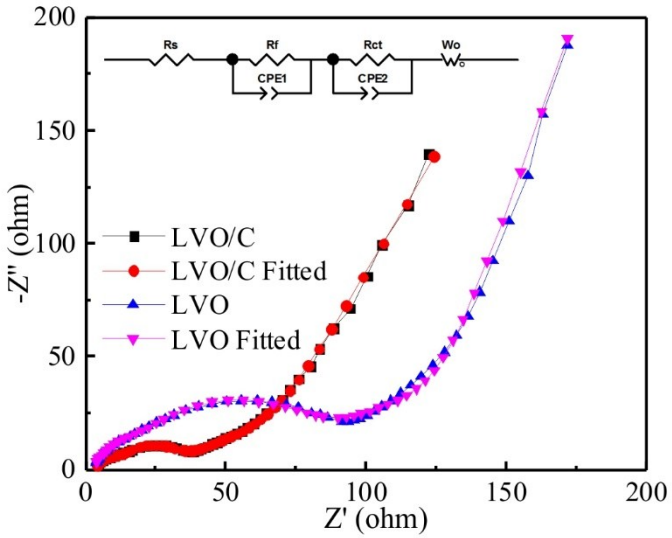

Figure S14. Nyquist plots of the LVO/C and LVO electrodes after 10 cycles.

References

1. K. Okuyama, M. Abdullah, I. W. Lenggoro and F. Iskandar, *Adv. Powder Technol.*, 2006, **17**, 587-611.
2. N. Tsapis, D. Bennett, B. Jackson, D. A. Weitz and D. A. Edwards, *PNAS*, 2002, **99**, 12001-12005.